Material extrusion of TPU: thermal characterization and effects of infill and extrusion temperature on voids, tensile strength and compressive properties

Manuel Sardinha
IDMEC, Instituto Superior Técnico, Universidade de Lisboa, Lisboa, Portugal
Luís Ferreira
IST, Instituto Superior Técnico, Universidade de Lisboa, Lisboa, Portugal
Hermínio Diogo
CQE, Instituto Superior Técnico, Universidade de Lisboa, Lisboa, Portugal
Tânia R.P. Ramos
CEGIST, Instituto Superior Técnico, Universidade de Lisboa, Lisboa, Portugal, and
Luís Reis and M. Fátima Vaz
IDMEC, Instituto Superior Técnico, Universidade de Lisboa, Lisboa, Portugal

Abstract

Purpose – This study aims to investigate the tensile strength and compressive behaviour of two thermoplastic polyurethane (TPU) filaments produced via material extrusion (ME): TPU 95A and Reciflex (recycled).

Design/methodology/approach – Tensile strength and compressive behaviour are assessed. The influence of extrusion temperature and infill pattern on these properties is examined, supported by thermal characterization, surface morphology analyses and a comprehensive comparison with existing literature. An analytical method is presented for estimating the solid ratio of ME parts, using an ellipse model to describe the material bead geometry.

Findings – Reciflex is generally stiffer than TPU 95A in both tensile and compressive tests. Specimens loaded orthogonally in compression tests exhibited stiffer behaviour than those loaded parallelly, and higher tensile properties were typically observed when material beads were deposited parallel to the load direction. Unlike TPU 95A, Reciflex is sensitive to extrusion temperature variations.

Social implications – By comparing recycled and virgin TPU filaments, this research addresses waste management concerns and advocates for environmentally sustainable production practices in the broadly used filament/based ME technique.

Originality/value – This study provides an extensive comparison of computed values with existing literature, offering insights into how different materials may behave under similar processing conditions. Given ongoing challenges in controlling melt flow during extrusion, these results may offer insights for optimizing the production of ME parts made with thermoplastic elastomers.

Keywords FFF, FDM, Beads, Fused deposition modelling, 3D printing, Fused filament fabrication, Porosity, Build direction, Raster

Paper type Research paper

1. Introduction

Additive manufacturing (AM), often referred to as 3D printing, encompasses a set of technologies that sequentially deposit or consolidate material, typically in a layer-by-layer manner (Gibson *et al.*, 2014). AM technologies allow the production of geometrically complex shapes and customized products, with potential gains in mechanical performance, cost reduction and environmental impact (Abdulhameed *et al.*, 2019; Lee *et al.*, 2017). Within the multitude of AM processes, filament-based material extrusion (ME) methods are among the most widely used for processing polymer materials, namely,

The current issue and full text archive of this journal is available on Emerald Insight at: **https://www.emerald.com/insight/1355-2546.htm**

Rapid Prototyping Journal
31/11 (2025) 62–81
Emerald Publishing Limited [ISSN 1355-2546]
[DOI 10.1108/RPJ-06-2024-0241]

Received 4 June 2024
Revised 22 October 2024
16 December 2024
Accepted 22 December 2024

thermoplastic elastomers (TPEs) (Awasthi and Banerjee, 2021; Zhou *et al.*, 2020).

TPEs commonly display both hard and soft phases, which is manifested by having rubber-like elasticity along with the processability commonly associated with thermoplastics (Nace *et al.*, 2021). Consequently, they can undergo repeated melting and processing without substantial loss of their properties, although the synthesis and processing conditions may influence their molecular structure (Awasthi and Banerjee, 2021). In addition, TPEs exhibit both amorphous and crystalline regions. Amorphous regions tend to lack a regular, ordered structure in their molecular chains, which contributes to the flexible properties of the material. In contrast, crystalline regions have an ordered molecular arrangement, contributing to the material's strength and rigidity (Babu and Naskar, 2010).

A filament-based ME system usually incorporates a feeder, a hot end and an extruder outlet (nozzle). The feeder directs the filament into the hot end, where the polymer is heated until it reaches a molten state, allowing it to be selectively deposited onto a build platform or onto previously deposited material (Altıparmak *et al.*, 2022). The feeder mechanism is either coupled to the hot end (direct drive extrusion) or mounted away from it, requiring a flexible tube to guide the filament to the hot end (Bowden extrusion). Typically, for flexible filaments, a direct drive extrusion system is preferred, as it minimizes the travel distance of the filament to the hot end, reducing the potential for filament clogging and promoting steady material throughput from the nozzle (Papazetis and Vosniakos, 2019). Despite significant advancements in ME technology over the past decade, several challenges persist (Qamar Tanveer *et al.*, 2022). Notably, there is still a need to enhance the accuracy of both process- and component-related simulations, as well as to understand how the technology can be scaled to meet the promises of mass customization for consumer products (Tofail *et al.*, 2018). Moreover, one of the key challenges is minimizing internal and surface defects while enhancing the mechanical properties of printed parts (Sardinha *et al.*, 2024; Wickramasinghe *et al.*, 2020).

In ME, build orientation refers to the position in which a printed object lies on the build platform during manufacturing, which defines how the layers are aligned within the object, and it is considered one of the most critical characteristics of these components (Coogan and Kazmer, 2020; Qamar Tanveer *et al.*, 2022). Infill refers to the material deposited within the walls of the printed part, and the raster angle can be defined as the angle at which the infill beads are deposited in relation to one principal direction of either the part or the machine. Build orientation and infill parameters such as raster angle justify the characteristic anisotropic behaviour of components and should be carefully considered when designing products (Koch *et al.*, 2017; Steuben *et al.*, 2015).

ME is typically a non-isothermal process with a cyclic, non-uniform thermal history that influences the final properties of components (Peng *et al.*, 2018). Both the extrusion temperature, which refers to the temperature of the hot end during extrusion, and parameters such as printing speed, layer height and outlet nozzle diameter directly affect volumetric material throughput (Coasey *et al.*, 2020; Mackay, 2018). During extrusion, processed thermoplastics exhibit viscoelastic behaviours, meaning they can combine both viscous flow and elastic deformation. Many of these materials are shear-thinning, where their viscosity decreases with increasing shear rate, though some may exhibit shear-thickening behaviour. In addition, ME parts can exhibit signs of residual stresses due to non-uniform cooling and shrinkage, as well as due to fluctuating shear and compression forces during the extrusion (Das *et al.*, 2021). Generally, slower printing speeds promote a stronger bonding of layers and infill beads, enhance geometrical tolerance and decrease the likelihood of print failure. At higher deposition rates, the material experiences pressure and temperature fluctuations inside the heating chamber, leading to an oscillating extrusion rate, which negatively impacts the final properties of the components (Ferraris *et al.*, 2019; Luo, 2020). Maintaining consistent values of storage modulus, loss modulus and complex viscosity is fundamental for achieving a uniform rheological response, which improves control over the flow behaviour of the melt (Das *et al.*, 2021). Extrusion temperatures that are 10°C–20°C higher than the material's melting temperature (T_m) generally provide adequate material viscosity for controlled deposition (Xiao and Gao, 2017). Bonding between adjacent beads and between layers (interlayer strength) is governed by coalescence processes, which results from phenomena such as surface wetting, neck growth and interfacial polymer chain diffusion and entanglements (Bellehumeur *et al.*, 2004; Coogan and Kazmer, 2017). Conduction is the dominant heat transfer mechanism in ME and because the bonding of material within a part is promoted by the thermal energy of the semi-molten deposited bead, the thermal history of the polymer plays a pivotal role in the quality of the bond (Bellehumeur *et al.*, 2004).

One impactful characteristic of extruded parts that deeply influences their mechanical properties is the presence of voids (Koch *et al.*, 2017; Sun *et al.*, 2023). In most cases, these voids are related to infill deposition strategies, occurring between adjacent materials beads and forming pathways or chimneys within the parts (Tao, Kong, *et al.*, 2021). Akhoundi and Behravesh (2019) investigated the influence of various infill strategies on the mechanical properties of ME parts, particularly focusing on the formation of voids. The study concluded that the highest tensile and flexural strength were significantly correlated with a reduction in void quantity. To minimize the presence of voids, Eiliat and Urbanic (2018) proposed a slicing method that generates raster orientations in each layer based on the geometry of the part. In addition to the infill deposition strategy, increasing the extrusion temperature has been reported to improve the flowability and reduce the viscosity during extrusion, reducing the number of voids found in parts (Wach *et al.*, 2018).

Concerning material-extruded thermoplastic elastomers (ME-TPEs), their applications span across diverse fields, including but not limited to uses in footwear, cushioning, tissue engineering and medical devices (Awasthi and Banerjee, 2021; Geng *et al.*, 2023). Recent advancements have expanded their utility into innovative areas such as acoustic dampers (Tao, Ren, *et al.*, 2021), orthotics (Mian *et al.*, 2024), flexible electronics (Papazetis and Vosniakos, 2019), soft robotics (Salem *et al.*, 2018) and non-pneumatic tires (Sardinha *et al.*, 2022, 2023). Nonetheless, the inherent soft nature of TPEs makes controlling the melt flow during extrusion particularly challenging, which can result in unpredictable and severe viscoelastic deformations (Awasthi and Banerjee, 2021). To avoid printing issues such as oozing and stringing effects, strategies that rely on tuning filament retraction and cooling, or carefully designing and positioning parts to limit travel movements within previously deposited paths, can promote printability and overall part quality (UltiMaker, 2024; Wu *et al.*, 2024). Still, printing parameters that enhance printability often conflict with those that ensure adequate mechanical integrity, requiring trade-offs (Ajinjeru *et al.*, 2017).

Thermoplastic polyurethanes (TPUs) are among the most common TPEs used in filament-based ME. Historically, they have been synthesized from petrochemicals, but can also be produced in a bio-based manner using plant oil–based polyols and diols (Datta and Kasprzyk, 2018). Moreover, in today's context, the use of recycled TPEs is an inevitable aspect of materials science. However, due to the intricate and variable compositions of thermoplastic and elastomeric components, the recycling of these materials presents significant challenges (Lin *et al.*, 2020). TPEs are composed of uneven molecular chain lengths requiring different energy amounts to activate. Because the different linkages in the polymer chain may have different thermal dissociation temperatures, reprocessing can lead to a loss of mechanical properties. In addition, thermal degradation of TPEs can begin between 110°C and 270°C, a range that falls within the temperatures used in ME (Zia *et al.*, 2007). Badini *et al.* (2024) tested the influence of extrusion temperature and infill on the tensile properties of two types of TPU (generic and recycled from tire rubber), focusing on the manufacturability and characteristics of the recycled material.

TPEs exhibit non-linear stress–strain behaviour, meaning there is no constant elastic modulus defining their complete elastic response, making it difficult to identify a yield point (Kucherskii, 2003; Treloar, 1975; Xu *et al.*, 2020). Despite this, two distinct elasticity regions are commonly observed: the initial region is associated with molecular disorder and randomness, often termed entropic elasticity, whereas the subsequent region occurs at higher strains, where the polymer chains are fully stretched, and is related to how the material stores and releases energy during deformation and recovery (Kartsovnik, 2022).

Because ME is a thermally activated extrusion process, it is crucial to have proper knowledge of the thermal characteristics of filaments, particularly the temperature at which filament material starts to melt, or the temperature range that defines brittle and elastic material behaviour, which is especially relevant when designing elastomeric components (Das *et al.*, 2021). Glass transition temperature (T_g) is a property of amorphous materials or the amorphous portion of a semi-crystalline material and defines the transitional temperature at which polymer segments start to move from a frozen state (with increasing temperature) or start to freeze (with decreasing temperature) (Bin Samsuri, 2017). As the temperature increases, and the polymer chains gain mobility, if there is sufficient energy to form ordered molecular arrangements, crystallization events can occur. Melting relates to the absorption of heat until molecular chains lose their ordered, solid structure, softening the polymer and making it gain the mobility associated with a viscous material, and is also linked with a sudden change in heat capacity (Frick and Rochman, 2004). T_g and T_m for amorphous and semi-crystalline polymers are usually not single, definite temperatures but ranges during which polymer molecular chains gain or lose mobility. Typically, elastomers are characterized by having very low T_g, which allows them to exhibit rubbery behaviour at ambient temperature.

In this work, the tensile strength and compressive behaviour of two ME-TPU filaments (recycled and generic TPU 95A) are studied, with a focus on how extrusion temperature and infill pattern influence these properties. Thermal characterization and surface morphology analyses are conducted to support the findings, and a comprehensive comparison of computed values with existing literature is performed. The research also explores the adequacy of an analytical method for estimating the solid ratio of parts. By correlating the estimated solid ratios with the actual voids, the research seeks to validate the method and explore its applicability. While there is some literature on the mechanical behaviour of ME-TPEs, several issues discussed above hinder the consistency in reporting their mechanical properties, limiting their applicability. Furthermore, there is limited information on important aspects such as the relationship between compressive load types, build orientation and mechanical properties. Therefore, this research advances material science within the rapidly evolving field of AM by clarifying the relationship between key ME process parameters and mechanical responses, thereby facilitating the design of elastomeric components.

2. Material and methods

The specimens produced for this experiment are divided into two main groups based on their shape and the mechanical test they are designed for: dog-bone specimens for tensile tests and cubic specimens for compression tests. Figure 1 provides an overview of how each specimen type is used in the different experimental procedures, which are detailed in the subsequent sections.

2.1. Thermoplastic polyurethanes

Among the several commercially available ME-TPE filaments, this work evaluates two TPUs: TPU 95A from Ultimaker® and Reciflex, a recycled filament from Recreus®. Ultimaker's TPU 95A is a widely used filament in ME and, according to research by (León-Calero *et al.*, 2021), consists of approximately 52% hard segments. Reciflex (Recreus, 2022) filament is made from recycled TPU, sourced from the footwear industry and Recreus' internal waste. Its hardness ranges between 92A and 98A, but limited additional data is available (Armstrong *et al.*, 2023). Table 1 summarizes the material characteristics reported by their manufacturers.

2.2. Production of test specimens

Figure 2(a) shows the geometrical features of the tensile specimens, which is designed to conform to both the Die C type specimens of American Society for Testing and Materials (ASTM) standard D412 (ASTM, 2016) and the type IV specimens of ASTM standard D638 (ASTM, 2014), with the exception of the width of the narrow section, which is 7.2 mm, a multiple of the nozzle diameter. The cubic specimens have a

Figure 1 Schematic of the production process and application of different specimen types in the research experiments

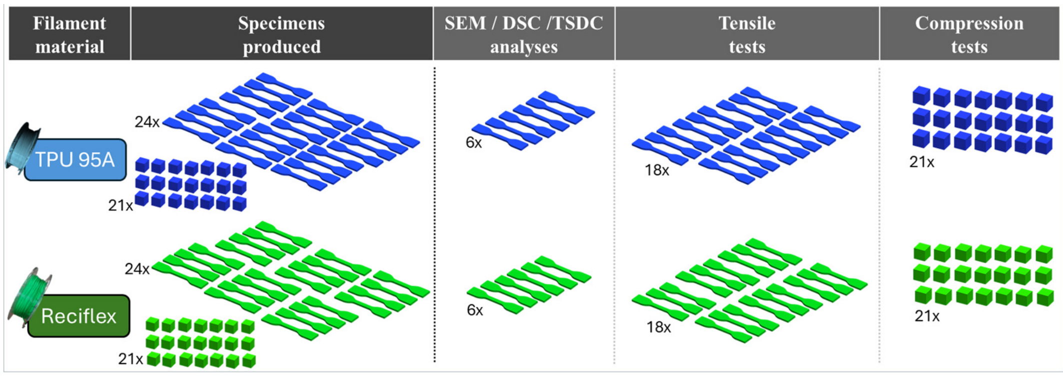

Source: Figure by authors

Table 1 Material characteristics of the materials, according to their manufacturers

Property, [units]	TPU 95A (UltiMaker, 2022)	Reciflex (Recreus, 2022)
Density (ρ), [g/cm^3]	1.22	1.00–1.22
Hardness (H)	96A/48D	92A–98A
Elongation at break (ε_R), [%]	>560[a]	>400
Young modulus [MPa]	61–73[a]	NA
Tensile strength [MPa]	22–40[a]	40 – 50

Notes: NA = not available; [a]For specimens produced lying flat on the build platform
Source: Table by authors

side length of 10 mm, selected to allow testing in different load directions. The Ultimaker S5, equipped with a Bowden-type extruder, was used to produce all specimens. The slicer software used to generate the G-code files was Ultimaker Cura version 4.11.0. All samples were manufactured with 100% infill, a layer height of 0.2 mm, a nozzle diameter of 0.4 mm, a line width of 0.38 mm and a printing speed of 30 mm/s. No top or bottom layers were applied; thus, all layers consisted of two outer walls and infill. In addition, a 0.4 mm overlap between the walls and the infill was used, and infill line beads were produced before the walls [Figure 2(b)]. Regarding the importance of temperature during production, the build platform and filament cooling fan were maintained at 50°C and 20% speed, respectively, with a minimum layer time of 15 s. Furthermore, this study evaluates the influence of three levels of extrusion temperature (per material) and three infill patterns. Four identical samples of each studied parameter were produced in a common printing session, one at a time. Before defining the extrusion temperatures, temperature towers for each material were produced, with 5°C increments between each level, Figure 2(c) and (d).

Temperature towers are used for the initial screening of extrusion temperatures, helping to identify suitable temperature ranges by assessing the printer's ability to reproduce features like bridges and overhangs and through visual inspection of interlayer adhesion. However, for these TPUs, only small differences between the tower's levels were observed. In the temperature tower test of TPU 95A, the material printed at 245°C exhibits not only a more pronounced stringing effect but also a subtle colour difference between the layers, which may indicate material degradation. In the temperature tower of Reciflex, no visible difference was observed in the material printed between 220°C and 230°C, but signs of under-extrusion and slight roughness were noted at 215°C, and signs of material oozing and colour variation appeared at 235°C. After this visual assessment, and considering results from previously published works (Sardinha *et al.*, 2024), thermal characterization performed (subsection 2.4), and a review of temperatures used in other studies, the chosen tested temperatures for TPU 95A were 225°C, 235°C and 240°C, and for Reciflex were 220°C, 225°C and 230°C.

Regarding the tested infill strategies, both linear and concentric types were studied, with three variations of raster angle orientations for the linear infill: [0°/90°], [45°/−45°] and [0°/0°]. Representative examples of these cubic specimens are shown in Figure 3(a)–(d).

2.3. Tensile and compression tests

Tensile and compression tests were performed using a universal testing machine Instron 5566 with a 10 kN load cell, at room temperature (21°C) and approximately 60% relative humidity. Considering previous research findings on the strain sensitivity of TPEs (Sean Teller, 2019; Vidakis *et al.*, 2021; Wang *et al.*, 2023), and the recommendation of relevant standards, tests were conducted with a crosshead speed of 20 mm/min for tensile tests and 2 mm/min for compression.

For the tensile testing, the gauge section of each specimen was measured at three different locations to estimate the cross-sectional area of the unstrained specimen. After toe correction of the zero-strain point, in accordance with ASTM standard D412 (ASTM, 2016), the nominal stress at a specified elongation (σ_{xxx}) was calculated using the load required to reach that elongation (F_{xxx}) and the average cross-sectional area of the unstrained specimens. To compare the stiffness and strength with available literature, the authors compute the tensile strength (σ_R), the elongation at break (ε_R) and the initial elastic modulus at strains ranging from 1% to 5% (E_i).

Compression tests were conducted by imposing a total crosshead displacement of approximately 70% of the initial

Figure 2 Design and manufacturing of the test specimens

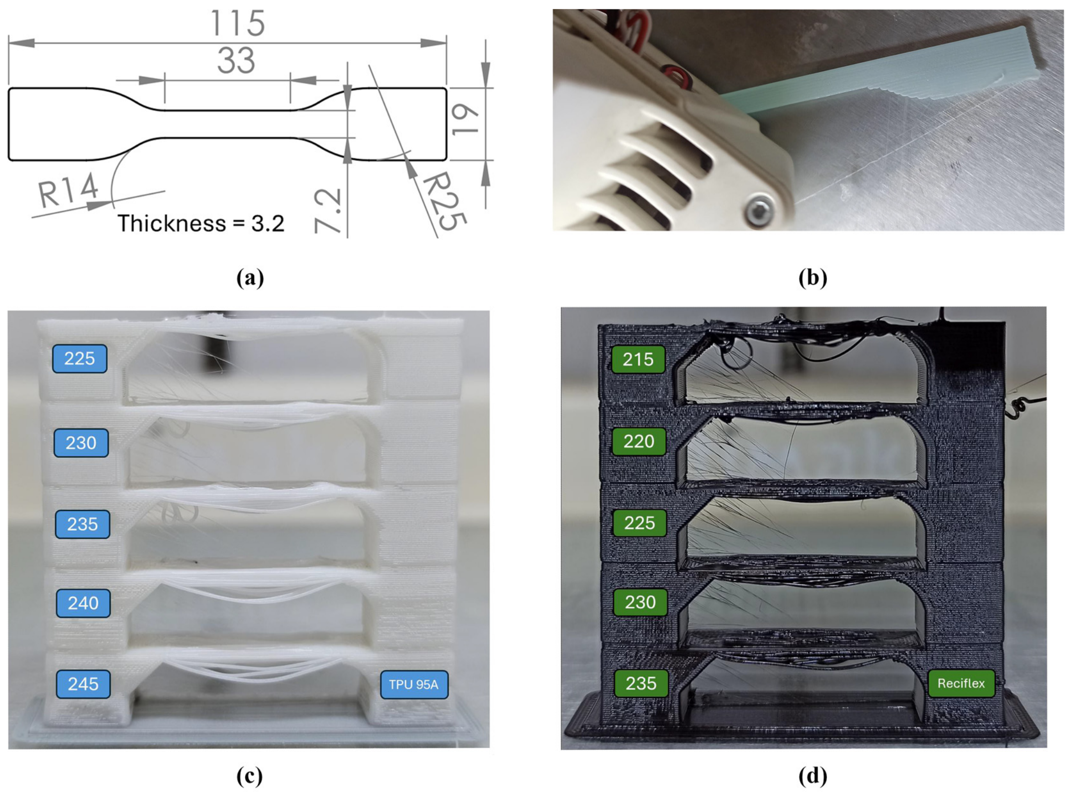

Notes: (a) Technical drawing of the tensile test specimens, with dimensions in millimetre; (b) First layer printing of a tensile specimen made from TPU 95A; (c) Temperature tower for TPU 95A; (d) Temperature tower for Reciflex
Source: Figure by authors

height of the specimens. To compare compression properties, the authors computed the elastic modulus and nominal stress at strain levels of 10%, 20%, 50% and 70%. Before testing, the initial height (h_i) and compression area of each specimen were measured. In addition, the height recovery (R_e) of the cubic specimens was estimated by remeasuring their height two weeks after testing (h_2), as shown in equation (1):

$$R_e = \frac{h_i - h_2}{h_i} \times 100 \tag{1}$$

Compression specimens printed with a [0°/90°] infill were tested with the load applied orthogonal to the layer plane, as shown in Figure 4(a). To evaluate the influence of infill on compression behaviour, the load was applied parallel to the layer plane. Specimens with a [0°/0°] infill were loaded in two different directions, as illustrated in Figure 4(b) and (c). Notably, loading the concentric and linear specimens with a [45°/−45°] infill along these two perpendicular directions yields equivalent results. As a result, a total of seven compression load cases were performed for each material.

Table 2 summarizes the study variables for each mechanical test, including the nomenclature based on material, extrusion temperature (T_{ext}), infill pattern and, for compression specimens, the load direction.

2.4. Thermal characterization

In this work, differential scanning calorimetry (DSC) was used to characterize the materials. DSC is a thermal analysis technique that measures the temperature and heat flow associated with material transitions as a function of time and temperature. The outcome is usually a heat flux versus temperature plot, where glass transitions manifest as a step in the recorded signal, reflecting a change in the heat capacity of the sample material. In this work, T_g is computed through the DSC software using an average of the change in heat capacity. T_m and crystallization temperature (T_c) are identified as the minimum of the endothermic transition and the maximum of the exothermic transition, respectively. Table A1 in Section A of the supplementary files associated with this research outlines DSC parameters from literature used to characterize 3D-printed TPUs.

In this study, DSC is used for the thermal characterization of four material samples. Specifically, one sample was extracted from each filament used, whereas the remaining two were derived from tensile test specimens produced with each material. After being processed through ME, the cross section of the specimens was cut into a thin layer to obtain a representative material amount, i.e. a sum of material from each layer. The experimental procedure used during the DSC follows some recommendations of ASTM standard D3418 (ASTM, 2015) and was carried out on a TA 2920 calorimeter.

Figure 3 Slicing preview of the deposition of the last layer of a cubic specimen (in blue) on top of previous layers (in grey), with infill type

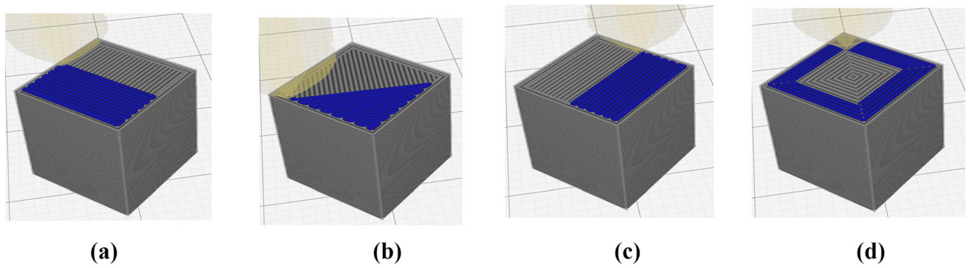

Notes: (a) Linear with a [0°/90°] orientation; (b) linear with a [45°/−45°] orientation; (c) linear with a [0°/0°] orientation; (d) concentric
Source: Figure by authors

Figure 4 Schematic of the load application in compression tests: the hexagonal yellow shape represents the extrusion head, the current layer is shown in blue and the previous layers are depicted in grey

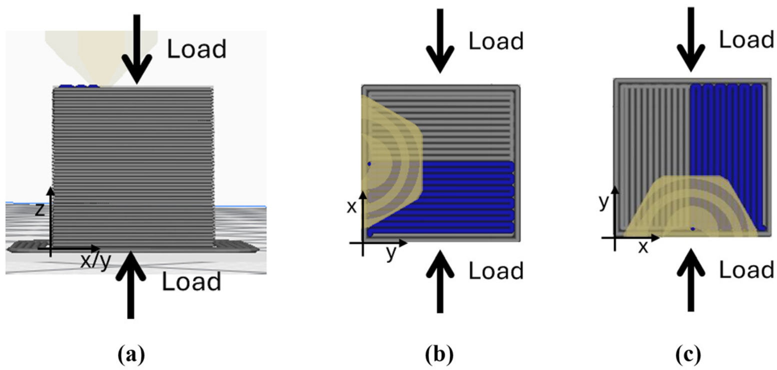

Notes: Load directions in specimens; (a) with [0°/90°] infill and load orthogonal to the layer stack; (b) with [0°/0°] infill and load orthogonal to infill beads; (c) with [0°/0°] infill and load parallel to infill beads
Source: Figure by authors

Table 2 Nomenclature and processing parameters for each batch of specimens

	Tensile specimens			Compression specimens		
Filament material	**Sample reference**	T_{ext} [°C]	**Infill pattern**	**Sample reference**	T_{ext} [°C]	**Infill pattern**
TPU	T1_TPU_T225_0_90	225	[0°/90°]	C1_TPU_T225_0_90_Z	225	[0°/90°]
	T2_TPU_T235_0_90	235	[0°/90°]	C2_TPU_T235_0_90_Z	235	[0°/90°]
	T3_TPU_T240_0_90	240	[0°/90°]	C3_TPU_T240_0_90_Z	240	[0°/90°]
	T4_TPU_T235_45_-45	235	[45°/−45°]	C4_TPU_T235_45_-45_XY	235	[45°/−45°]
	T5_TPU_T235_Concentric	235	Concentric	C5_TPU_T235_Concentric_XY	235	Concentric
	T6_TPU_T235_0_0	235	[0°/0°]	C6_TPU_T235_0_0_X	235	[0°/0°]
				C7_TPU_T235_0_0_Y	235	[0°/0°]
Reciflex	T7_Reci_T220_0_90	220	[0°/90°]	C8_Reci_T220_0_90_Z	220	[0°/90°]
	T8_Reci_T225_0_90	225	[0°/90°]	C9_Reci_T225_0_90_Z	225	[0°/90°]
	T9_Reci_T230_0_90	230	[0°/90°]	C10_Reci_T230_0_90_Z	230	[0°/90°]
	T10_Reci_T225_45_-45	225	[45°/−45°]	C11_Reci_T225_45_-45_XY	225	[45°/−45°]
	T11_Reci_T225_Concentric	225	Concentric	C12_Reci_T225_Concentric_XY	225	Concentric
	T12_Reci_T225_0_0	225	[0°/0°]	C13_Reci_T225_0_0_X	225	[0°/0°]
				C14_Reci_T225_0_0_Y	225	[0°/0°]

Source: Table by authors

The samples, ranging in mass from 7.9 to 11.3 mg, were weighed with a precision of ±0.1 μg using a Mettler UMT2 ultra-micro balance. Sealed aluminium crucibles with a perforated lid were used. The experiments were performed with a temperature range from −70°C to 250°C at a rate of 15°C/min, under a flow of high pure helium of 30 cm^3/min. The temperature scale of the instrument was calibrated at the same heating rate based on the fusion temperatures of indium and tin. The calibration of the heat flow scale was based on the area of the fusion peak and the enthalpy of fusion of the indium reference material.

Thermally stimulated depolarization current (TSDC) is a technique based on a sample's depolarization by thermal activation and can also be used to detect the T_g of polymers. TSDC can be very sensitive and affected by aspects like the structural, electrical, thermal and polarization characteristics of the samples. When performing this technique, at the polarization temperature (or poled temperature), a static electric field is applied to the sample for a sufficient time to allow various mobile entities to orient themselves within the field. This configuration is then fixed by rapidly decreasing the temperature while maintaining the electric field, preventing the relaxation of dipoles and/or charges. Once the temperature stabilizes, the electric field is switched off, and the sample is short-circuited for a specific period to eliminate any surface charges and stabilize the sample. Subsequently, the poled sample under an inert helium atmosphere is short-circuited and connected to a highly sensitive electrometer. The furnace containing the sample is then programmed to increase its temperature linearly over time. During this increase, the return to equilibrium of the previously oriented entities creates a depolarization current which is recorded as a function of temperature.

TSDC measurements were conducted by subjecting two samples, processed through ME, to electric polarization under an inert atmosphere. The process used a scanning temperature range from −80°C to 30°C, covering the glass transition region of un-poled samples (baseline) as well as samples poled at polarization temperatures of −20°C for TPU and 5°C for Reciflex. The strength of the polarizing electric field used was 200 V/mm, with a polarization time of 5 min. The freezing temperature was set to −80°C, and the heating rate was 8 K/min. Additional physical background of the TSDC technique and a deeper explanation of the experimental procedures used can be found in Diogo *et al.* (2016).

2.5. Geometrical structure analysis

Un-tested specimens were visually inspected using a Velleman® digital microscope, model CAMCOLMS1N, to identify macroscopic production defects. In addition, scanning electron microscopy (SEM) was used to assess the bonding quality resulting from each studied parameter by observing the cross sections of tensile test specimens, using the Phenom ProX G6 model from Thermo Fisher Scientific (Waltham, MA, USA). Figure 5(a) shows a representation of the cross section analysed and its approximate location within the gauge section of a tensile specimen. To prepare the samples, specimens were placed in a cooling chamber at −80°C for 72 h, as represented in Figure 5(b), and then cut with a sharp blade. Because TPUs are non-conductive polymers, a coating of gold and palladium was applied for SEM analysis, as seen in Figure 5(c).

Figure 5 Representation of important steps of the SEM analysis

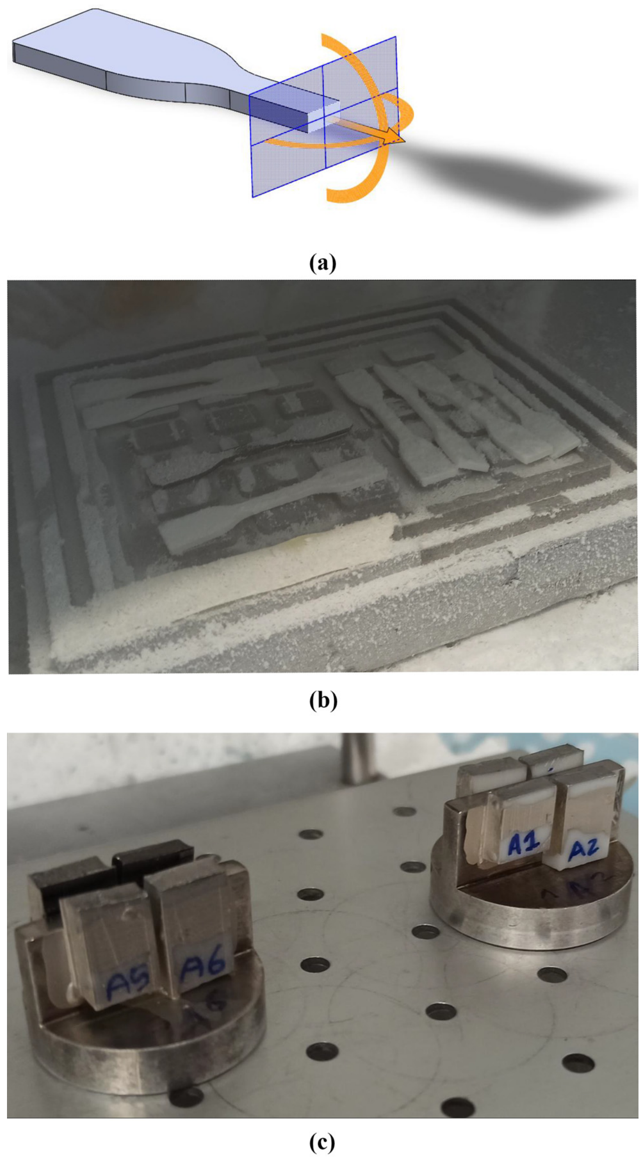

Notes: (a) Model of a tensile test specimens with the section cut at half its length showing the observed plane of the analysis; (b) Tensile test specimens being removed from the cooling chamber; (c) SEM specimen carrier with coated material samples mounted
Source: Figure by authors

By examining the SEM images of the cross sections, it is possible to observe and quantify voids within parts. These voids typically manifest as irregular-shaped pathways in the specimen's structure because they represent air gaps between adjacent beads. This analysis enables inference about the relationship between the bonding quality between beads and the mechanical properties of each specimen. Stronger parts are typically correlated with beads printed closely together which, in theory, minimizes voids within parts. The distance between infill beads is influenced by manufacturing parameters such as the line width, the overlap between infill paths and overall material flow. Even though material is extruded through a circular nozzle, the flow of extruded material is shaped by the interaction between the nozzle and the printing substrate, which causes the cross-sectional geometry of each bead to approximate an elliptical shape (Wang *et al.*, 2023). Therefore, a theoretical solid ratio (SR) of ME parts can be defined as the ratio between the area of consolidated beads (A_{bead}) and the maximum bead area [equation (2)]:

$$SR = \frac{A_{bead}}{A_{max}} \tag{2}$$

Computing the area of a consolidated bead often takes into account thermo-structural conditions that define the bonding phenomena between materials (e.g. surface diffusion and material viscosity), as proposed by Garzon-Hernandez *et al.* (2020). However, simple analytical models based solely on the geometry of deposited beads provide a fast and practical estimation of the SR. Based on a proposal of Koch *et al.* (2017), the area of a consolidated bead can be defined as the area of an ellipse (A_{ellipse}), where the semi-major (a) and semi-minor (b) axes correspond to the layer height (h) and line width (d) of the extrusion process, respectively, allowing the SR to be computed using equation (3):

$$SR_{Koch} = \frac{A_{ellipse}}{A_{max}} = \frac{ab\pi}{hd} = \frac{\pi}{4} \cong 0.785 \tag{3}$$

Clearly, defining the bead shape as a simple ellipse would be a very conservative approach. An analytical model that better defines the geometry of adjacent beads, with no overlapping deposition paths, can be more accurately expressed by considering this shape as a minimum SR. As the process evolves, the ellipse grows within a bounding box whose size is defined by the layer height and line width, as illustrated in Figure 6.

In this model, the consolidated bead area is given by the sum of the three shaded areas shown in the schematic, and the SR can be computed using equation (4):

Figure 6 Schematic of the analytical method to estimate the SR, based on ellipsoidal-shaped filament beads

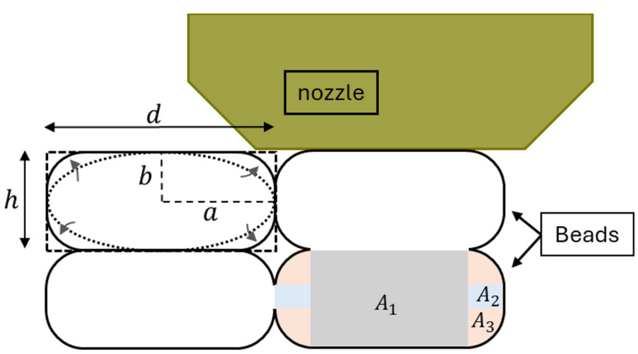

Source: Figure by authors

$$SR = \frac{A_1 + 2A_2 + 4A_3}{A_{max}} = \frac{h(d-2a) + 2a(h-2b) + ab\pi}{hd} = \frac{hd + ab(\pi - 4)}{hd} \tag{4}$$

To assess the adequacy of this estimate, the normalized density of test specimens was computed by analysing the area ratio between the solid and pore regions from cross-sectional SEM images. ImageJ software was used to quantify the size of inter-bead voids within each specimen's cross section. It should be noted that the normalized density is an average density computed using a representative area of the specimen and does not account for localized effects or void variations in the walls and centreline of the specimens.

3. Results and discussion

3.1. Thermal characterization

Figure 7(a) and (b), displays the endothermic and exothermic evolutions of the DSC analysis of both filament (un-processed) and ME-processed form. The results show marginal differences, suggesting that the ME process does not significantly affect the material's thermal properties, and that the T_g range of both materials is broad, which is characteristic of amorphous and semi-crystalline polymers, as it is a second-order transition. The remaining heating and cooling cycles are available in the supplementary files (Section A).

After being processed by ME, the range of glass transition decreases by 6°C in the TPU 95A and 8.1°C in the Reciflex. However, while the T_g of TPU 95A increases after processing, the opposite occurs in Reciflex. After being processed, the melting peak of both materials decreases approximately 14°C. The cooling traces of all samples exhibit similar trends. Nevertheless, unlike Reciflex, two distinct peaks can be observed in TPU 95A when the sample cools from 250°C. This exothermic signature is associated with crystallization temperatures (T_c). This phenomenon suggests that, after material deposition, when reaching such temperatures, crystallization might occur, potentially influencing the bonding with subsequent layers.

Notably, the two lowest temperatures used in the temperature tower tests are below the melting peaks identified in these samples. This suggests that the energy provided to the materials during extrusion at these temperatures may not be sufficient to properly activate the polymer chains, potentially affecting the steadiness and controllability of melt flow during extrusion and influencing the mechanical properties

Figure 8(a) and (b), displays the results of the molecular motions study conducted using the TSDC technique. Analysis of the thermogram reveals the presence of two distinct mobilities, with moderate overlap but varying intensities. For TPU 95A, the peak temperatures are recorded at −24.7°C and 6.8°C, whereas for the Reciflex material, they occur at −26.1°C and 5.8°C. The similarity in the curve shapes and the proximity of the peak temperatures within the covered temperature range suggest comparable structural characteristics between the two materials. In addition, for both samples, the mobility characteristics observed at the lowest temperature indicate the signature of the glass transition temperature as detected by the TSC technique.

Figure 7 DSC-measured heat flow during

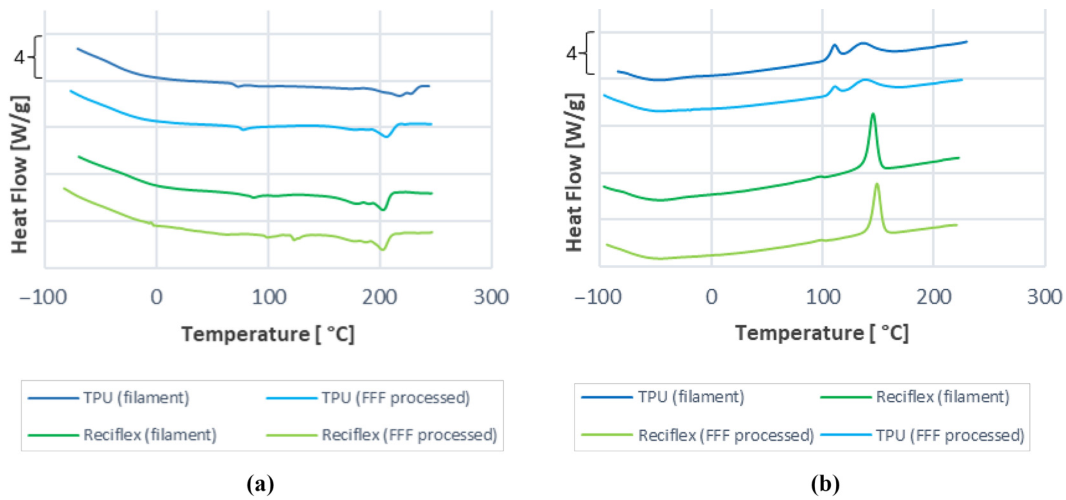

Notes: (a) First heating (endothermic); (b) second cooling (exothermic)
Source: Figure by authors

Figure 8 Thermogram from the TSDC analysis of both materials processed through ME

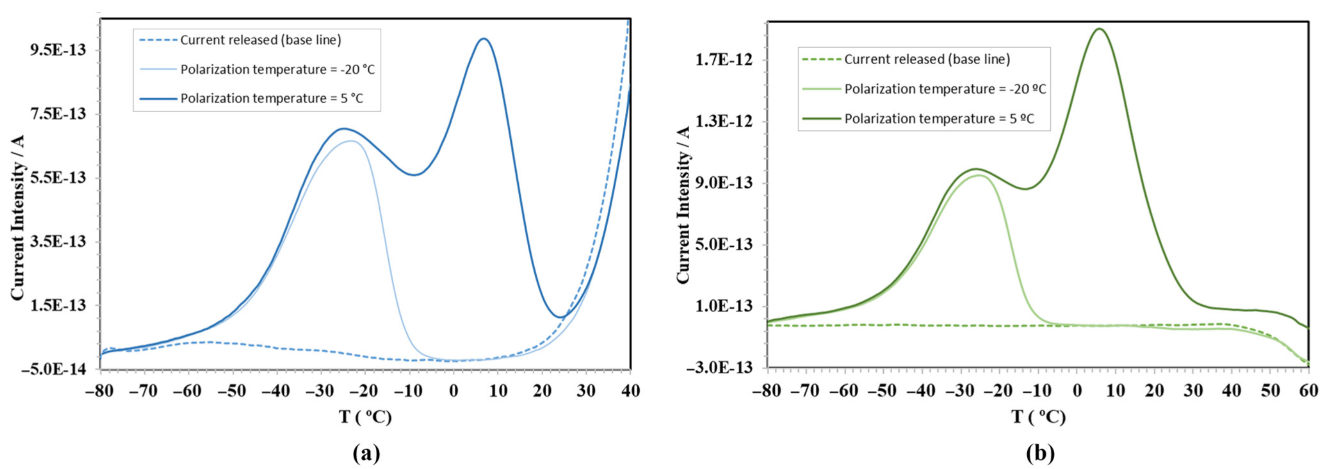

Notes: (a) TPU 95A; (b) reciflex
Source: Figure by authors

Table 3 summarizes the main thermal characteristics of each material. A comparison of the obtained results with available literature shows that the identified values of the T_g and a T_m for TPU 95A align with the findings of León-Calero *et al.* (2021), which reported a T_g between −54°C and −34°C, and a T_m of approximately 220°C. Furthermore, the identified T_m of the TPU 95A samples approaches the values reported in the data sheet of the material (216.8°C) (UltiMaker, 2022). No reported values were found for Reciflex.

3.2. Surface morphology

Figure 9(a)–(f) depicts representative surface morphologies obtained through SEM analysis. Additional images of each observed surface can be found in the supplementary files (Section B). Voids between deposited infill beads are visible in all specimens. Figure 9(a) shows the cross section of a TPU 95A specimen printed at 235°C with a [0°/0°] infill, including representations of approximate bead shapes. The magnified view of this cross section, in Figure 9(b), facilitates the identification of two types of defects observed in the specimens: inter-bead voids and air pores. Air pores were not included in further analysis, as inter-bead voids are more prevalent and larger in size.

Figure 9(c) shows the edge of the cross section of a TPU 95A specimen printed at 225°C with a [0°/90°] infill, which allows the identification of the layer height used in printing. Despite the 0.4 mm overlap used between the outer walls and the infill, smaller and more irregular voids remain visible between these two types of beads.

As anticipated, identifying differences in specimens with concentric and linear [0°/0°] infills can be challenging.

Table 3 Thermal characteristics (T_g, T_c and T_m) of tested material samples

Testing sample	Condition	T_{ext} [°C]	TSDC T_g [°C]	DSC T_g [°C]	DSC T_c [°C]	DSC T_m [°C]
TPU 95A	Filament	–	–	[−45.9; −19.7]	110.8/137.2	227.8
	ME processed	235	−24.7	[−41.2; −12.9]	111.3/138.7	214.3
Reciflex	Filament	–	–	[−30.4; −2.1]	145.4	216.5
	ME processed	225	−26.1	[−36.2, −16.0]	149.0	202.7

Source: Table by authors

Figure 9 Representative SEM images of the surface morphology of the cross section of specimens, with dimensions in micrometre

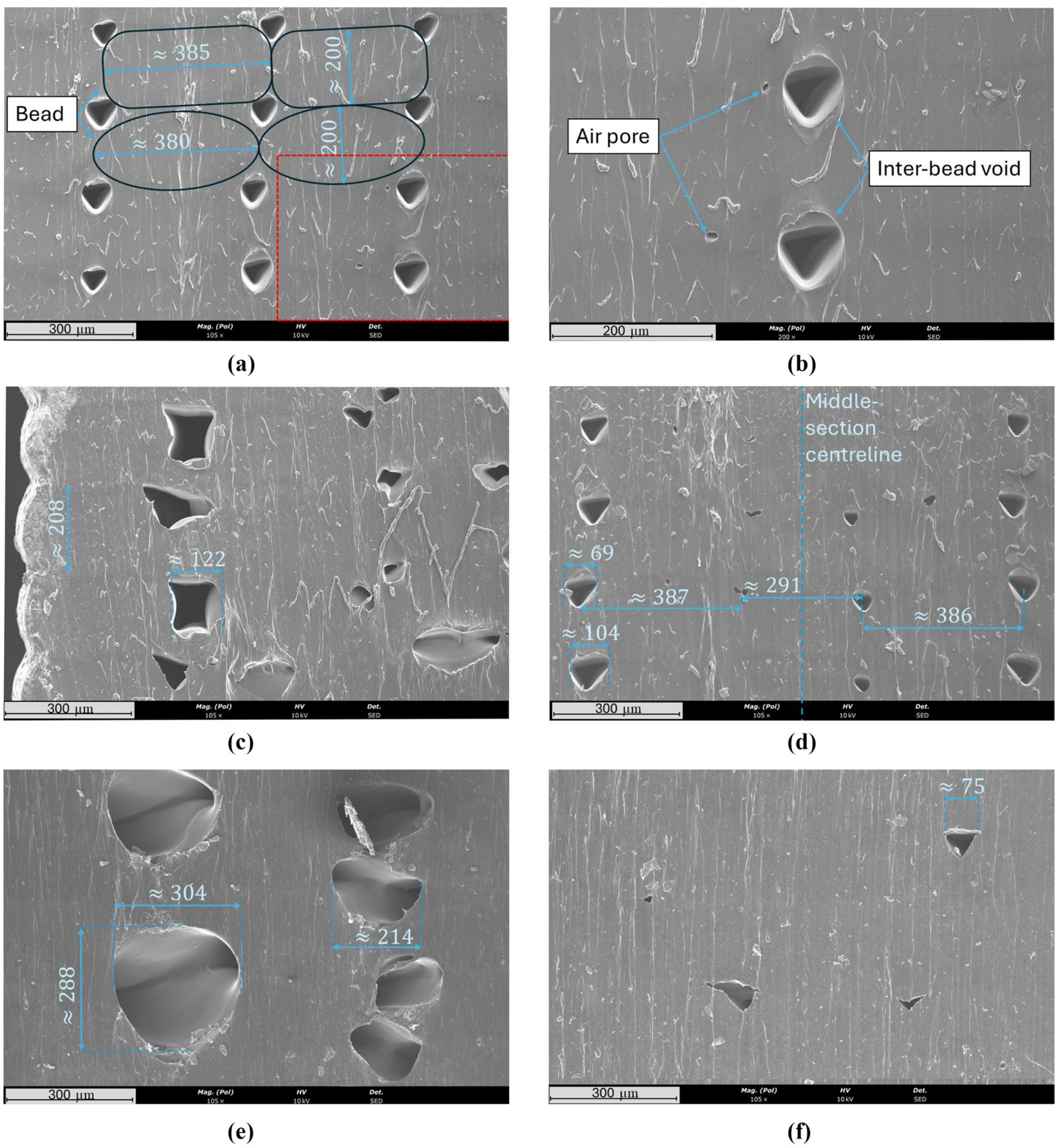

Notes: (a) T6_TPU_T235_0_0 with bead schematic and an area of magnification (in red); (b) magnified view of the T6_TPU_T235_0_0, showing different types of defects; (c) edge of a T1_TPU_225_0_90 specimen; (d) centre of a T5_TPU_235_concentric specimen; (e) T10_Reci_225_45_45; (f) T9_Reci_230_0_90
Source: Figure by authors

Compared to the [0°/0°] infills, specimens with a [0°/90°] infill exhibit approximately half the number of voids. This reduction may be attributed to the fact that half of the layers are deposited parallel to the cross-sectional view plane. The surface section in Figure 9(d) exemplifies the middle of the cross section of the specimens with concentric infill, where a reduction in the number of voids near the cross-sectional centreline is observed. This observation may be attributed to the fact that the narrow section of the tensile specimens with concentric infill consists of layers with 19 parallel infill lines, each with a width of 0.38 mm (totalling 7.22 mm). In addition, the infill deposition starts from the outer edge. Considering the narrow section of the specimens is only 7.2 mm wide, despite potential flow adjustments through software compensation, the last deposited infill line must fit into a smaller gap between previously deposited infill material.

The surface morphology of a Reciflex specimen with a linear [45°/−45°] infill, as shown in Figure 9(e), reveals that, from a cross-sectional perspective, this infill orientation generates ovalized and larger voids. Furthermore, the image also shows that, in some cases, larger voids result from the merging of voids from two consecutive layers deposited orthogonally to each other. Apart from these, and voids near the specimens' walls, the shape of most voids observed in this work aligns with the triangular voids detailed in the review by Sun *et al.* (2023).

Figure 9(f) exemplifies how higher temperatures result in smaller and less frequent voids across specimens, and Table 4 summarizes the average size of inter-bead voids, as well as the software-measured SR. Notably, in Reciflex, increasing the extrusion temperature from 220°C to 230°C led to a reduction in the average void size from 0.024 to 0.002 mm^2. Similarly, in TPU 95A, a wider temperature range (15°C) caused a decrease in average void size from 0.006 to 0.001 mm^2. The measured SR, which is directly linked to void size and frequency, reached its highest values when specimens were produced at the highest tested temperatures, namely, 0.993 in Reciflex and 0.983 in TPU 95A. This trend aligns with previous studies on the effect of increasing extrusion temperature in the reduction of voids (Elhattab *et al.*, 2022; Kasmi *et al.*, 2022; Wach *et al.*, 2018), most likely due to an increased flowability and reduced viscosity of the extruded material. Even so, it is expected that the higher flowability during extrusion may affect the dimensional accuracy of parts (Sun *et al.*, 2023).

Table 4 Summary of average void size and software-measured SR of each analysed study variable

Reference sample	Measured SR	Average void size [mm^2]
TPU 95A		
T1_TPU_T225_0_90	0.906	0.006 ± 0.005
T2_TPU_T235_0_90	0.950	0.006 ± 0.002
T3_TPU_T240_0_90	0.983	0.001 ± 0.001
T4_TPU_T235_45_-45	0.965	0.004 ± 0.001
T5_TPU_T235_Concentric	0.952	0.004 ± 0.001
T6_TPU_T235_0_0	0.960	0.003 ± 0.001
Reciflex		
T7_Reci_T220_0_90	0.789	0.024 ± 0.018
T8_Reci_T225_0_90	0.910	0.014 ± 0.009
T9_Reci_T230_0_90	0.993	0.002 ± 0.001
T10_Reci_T225_45_-45	0.779	0.034 ± 0.020
T11_Reci_T225_Concentric	0.965	0.002 ± 0.001
T12_Reci_T225_0_0	0.960	0.003 ± 0.001

Source: Table by authors

Figure 10 shows the relationship between the measured SR of specimens and the analytical approach based on the ellipse constrained by layer height and line width. In most tested cases, the ellipse model provides an adequate description of void presence, except for Reciflex specimens produced at the lowest temperature or with a linear [45°/−45°] infill. The model is more accurate at lower SR values, but as SR approaches 0.9, the influence of triangular void shapes increases, making precise predictions more challenging. If the two Reciflex outliers are excluded, the measured SRs range from 0.906 to 0.983 for TPU 95A and from 0.910 to 0.993 for Reciflex. These values are comparable to the results reported by Wang *et al.*, 2023), who reported an SR range of 0.93–0.97 for five different 3D-printed TPEs. In summary, this analysis suggests good bonding between adjacent beads because, aside from void location, it is difficult to identify layer stratification or distinct bead boundaries, almost independently of the process parameters used.

3.3. Tensile properties

Figure 11 allows for a comparison of the tensile properties of each material, with each curve representing the average of three specimens. Notably, the shape of the tensile stress–strain curves obtained in the present study differs considerably from those observed in other polymers, such as polylactic acid (Adibeig *et al.*, 2023). As expected, these materials exhibit hyperelastic behaviour, undergo significant elastic deformation and display a non-linear stress–strain relationship, which is evident from changes in the slope during loading. The complete set of individual tensile results can be found in the Section C of the supplementary files. A general visual analysis of these results shows that, in terms of stiffness and energy absorption capabilities, the Reciflex material is slightly superior across variations in production parameters, except for the specimens printed at 220°C. Consistent with existing research, no clearly discernible yield point is observed in the material behaviour. However, it can be noted that a transition between the two main elasticity domains typically occurs between strains of 15% and 30%, at a nominal stress of 5–10 MPa.

Figure 12(a) and (b), compares the average tensile strength (σ_R) and the elongation at break (ε_R), respectively. When analysing the effect of extrusion temperatures on strength and stretchability, both materials exhibit minor differences in specimens produced at the two highest temperatures, whereas the lowest temperature consistently resulted in the weakest mechanical properties.

Regarding infill strategies, the first specimens fail after approximately 200% elongation, with the highest stretchability reaching roughly 500%. Notably, concentric infill consistently results in the lowest strength and stretchability, and individual tests revealed a premature and erratic failure behaviour. The authors hypothesize that this may be due to gaps generated by inaccuracies in the slicing procedure, as seen in the slicer preview of Figure 13(a). A visual inspection of these specimens'

Figure 10 Comparison between the measured SR and analytical method for bead shape, based on ellipse model constrained by layer heigh and line width

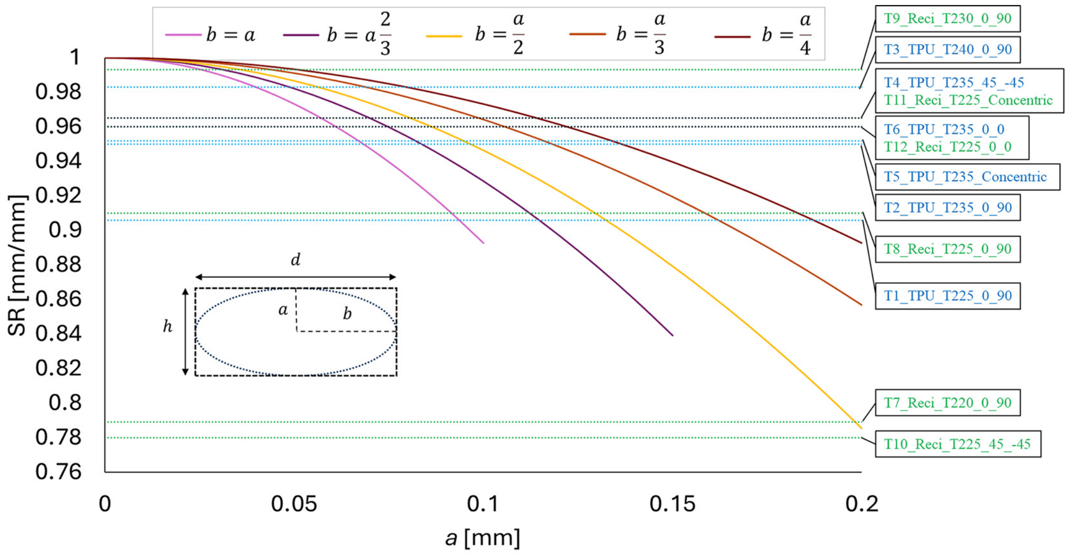

Source: Figure by authors

Figure 11 Nominal stress–strain plot of the tensile tests performed on TPU 95A (blue) and Reciflex (green)

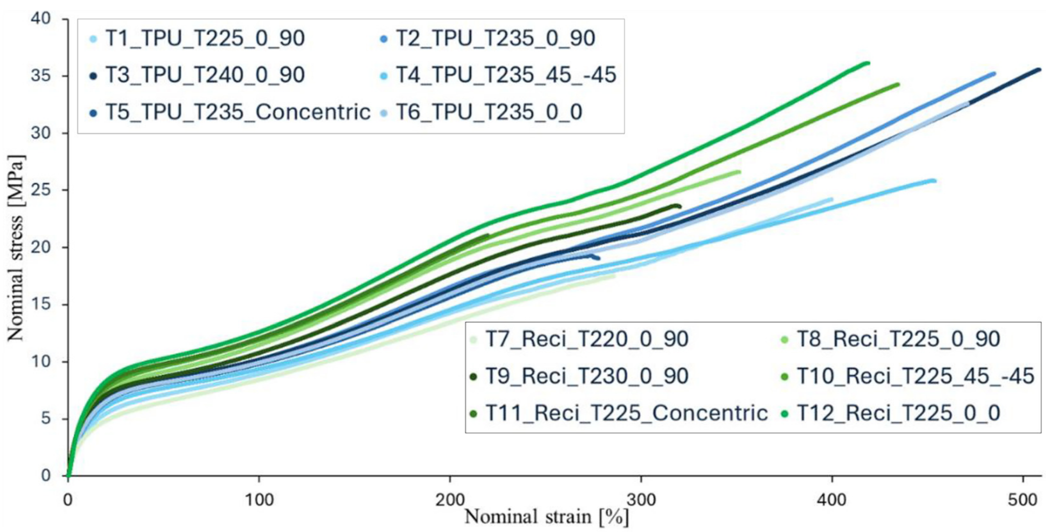

Notes: For each study variable, the plotted curve represents the average result of a batch of specimens
Source: Figure by authors

top layers confirms the presence of a defect that extends through the thickness of the specimen, likely marking the fracture initiation. Overall, most specimens displayed signs of both inter- and intra-layer fractures near the fractured surface zone, which showed a significant reduction in cross-sectional area.

Figure 13(b) compares the initial elastic modulus computed for each specimen. Results show that increasing the extrusion temperature from 225°C to 235°C and 240°C resulted in TPU 95A becoming roughly 30% stiffer. For Reciflex, increasing the extrusion temperature from 220°C to 225°C resulted in more than a 50% increase in initial stiffness, but an additional 5°C increment reduced the stiffness. Comparing the results of specimens with different infill shows that the initial elastic modulus of Reciflex is maximized in those with [0°/0°] infill, followed closely by those with concentric infill. In contrast, infill strategies had a minor influence on the initial elastic modulus of TPU 95A, though it is also maximized in specimens with concentric and [0°/0°] infill.

Overall, the behaviour observed for TPU 95A falls within the range of values reported in the literature for 3D-printed TPU

Figure 12 Tensile properties of tested specimens

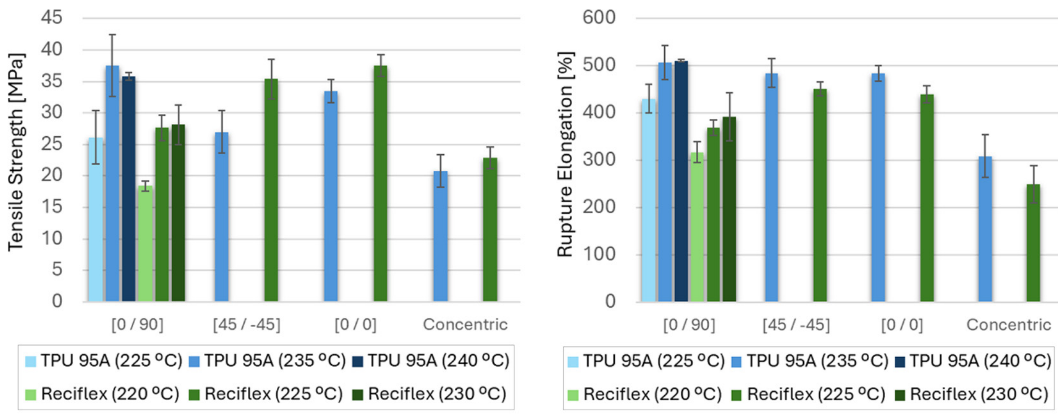

(a) **(b)**

Notes: (a) Tensile strength (σ_R); (b) elongation at break (ε_R)
Source: Figure by authors

Figure 13 (a) Illustration of a macroscopic production defect in specimens with concentric infill; (b) Initial elastic modulus (E_i) of tested specimens

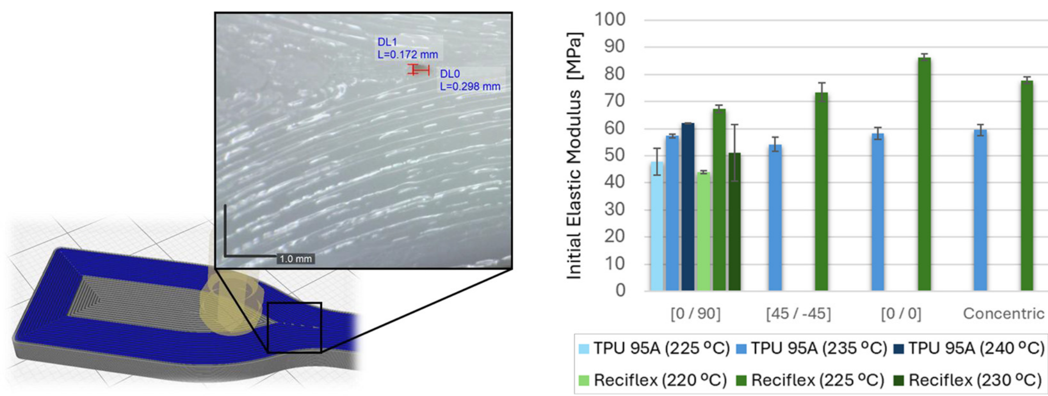

(a) **(b)**

Notes: The slicing preview shows the current deposited layer (in blue), alongside a magnified view of the top layer of an untested specimen, highlighting a macroscopic defect through the specimen's thickness
Source: Figure by authors

95A (Mian *et al.*, 2024; Xiao and Gao, 2017), and is comparable to existing reports on other TPUs. Regarding the Reciflex filament, limited information is available beyond the manufacturer's data. Nevertheless, Reciflex demonstrates behaviour very similar to TPU 95A, and its strength and stiffness can be easily compared to TPUs tested in similar studies. Badini *et al.* (2024) compared the behaviour of a recycled TPE (made from waste tire rubber) with TPU 80A, finding the recycled material to be approximately twice as stiff as TPU 80A. However, the rubber-based filament did not exhibit the same sensitivity to extrusion temperature changes as the Reciflex filament used in this study. Table 5 summarizes the available literature on the tensile properties of various types of 3D-printed TPUs, along with the computed values for initial elastic modulus, tensile strength and stretchability from this research.

Although drawing a general conclusion is challenging due to some outliers and unknown sources of variation, the maximum strength and stiffness are primarily observed in material beads deposited parallel to the load direction, notably in specimens with a [0°/0°] infill. This observation aligns with existing literature on ME (Qamar Tanveer *et al.*, 2022). For instance, Arifvianto *et al.* (2021) tested 3D-printed TPU specimens using various infill strategies and found that strength and stiffness are maximized in specimens with [0°/0°] infill. Similarly, Kasmi *et al.* (2022) observed improved mechanical response in specimens with the same infill orientation.

Table 5 Summary of tensile properties of tested specimens and available literature reports

Source	TPU type	Test speed [mm/min]	E_i [MPa]	σ_R [MPa]	ε_R [%]	T_{ext} [°C]	Infill type
Arifvianto *et al.* (2021)	Generic	5	28–38	19–41	400–600	190/200/210/220/230	[0°/0°]; [45°/−45°]; [0°/90°]; [30°/30°]; [60°/60°]; [90°/90°]
Xiao and Gao (2017)	Tecoflex LM-95A	500	NA	31–47	591–702	200/215/230	[45°/−45°]; [0°/90°]
Kechagias *et al.* (2021)	Ravathane® 140 D70	10	40–75	16–32	250–600	205/215/225	[45°/−45°]
Vidakis *et al.* (2021)	Ravathane® 140 D70	10, 50, 100, 200, 300	45–100	14–27	150–400	205/215/225	[45°/−45°]
Mian *et al.* (2024)	Raise3D TPU 95A	5 and 200	NA	28	350	250	[45°/−45°]
Kasmi *et al.* (2022)	Pollen AM	5	11–18	12–22	250–950	230/240/250	[0°/0°]; [45°/−45°]; [0°/90°]; [90°/90°]
Hohimer *et al.* (2017)	Elastollan 1185A	10	NA	20–40	450–550	190/205/220	[0°/0°]; [45°/45°]; [90°/90°]
Badini *et al.* (2024)	Generic TPU 80A	50	25–30	NA	NA	220/230/240	[0°/0°]; [0°/90°]; [90°/90°]
This research	Ultimaker TPU 95A	20	47.9 ± 4.8	26.1 ± 4.2	430.2 ± 30.4	225	[0°/90°]
			57.3 ± 0.6	37.5 ± 4.9	507.0 ± 35.5	235	[0°/90°]
			62.0 ± 0.1	35.8 ± 0.6	511.2 ± 2.6	240	[0°/90°]
			54.2 ± 2.6	27.0 ± 3.4	484.8 ± 30.5	235	[45°/−45°]
			59.6 ± 2.0	20.8 ± 2.6	308.6 ± 45.0	235	[Concentric]
			58.2 ± 2.1	33.5 ± 1.9	484.5 ± 16.4	235	[0°/0°]
	Recreus Reciflex	20	43.9 ± 0.6	18.4 ± 0.8	317.4 ± 21.8	220	[0°/90°]
			67.4 ± 1.4	27.6 ± 2.1	369.7 ± 16.5	225	[0°/90°]
			51.1 ± 10.6	28.1 ± 3.2	392.5 ± 51.3	230	[0°/90°]
			73.4 ± 3.3	35.4 ± 3.2	451.1 ± 14.6	225	[45°/−45°]
			77.8 ± 1.2	24.1 ± 0.4	389.8 ± 15.6	225	[Concentric]
			86.3 ± 1.2	37.5 ± 1.7	439.8 ± 18.7	225	[0°/0°]

Source: Table by authors

Rapid Prototyping Journal
Volume 31 · Number 11 · 2025 · 62–81

The correlation between the results and the measured SR of specimens varies. Strength and stretchability show a weak correlation with computed SR values across different infills for both materials. However, in TPU, a slight correlation between stiffness and computed SR is observed. When focusing on extrusion temperature, a slight positive correlation between an increase in SR and improvements in strength and stretchability, particularly in the Reciflex material. This observation corroborates some of the findings by Hohimer *et al.* (2017), which state that voids significantly impact strength. Nevertheless, our results suggest that further studies are needed to fully understand these phenomena.

3.4. Compressive properties

Figure 14(a) and (b), shows the nominal compression stress–strain behaviour of TPU 95A and Reciflex, respectively. The complete set of individual compression results can be found in the supplementary files (Section D). Overall, the plots indicate that variations in loading direction, infill and temperature parameters have limited influence on the results, except for Reciflex, which is sensitive to changes in extrusion temperature. Excluding the two temperature extremes, this recycled material consistently exhibits higher compression stiffness compared to TPU 95A.

Table 6 summarizes the computed averages and standard deviations of initial compression stiffness (from 1% to 20% strain), stress values at various strains and height recovery (R_e) for each batch of compression specimens. Comparing the relationship between infill strategies and load direction, as anticipated, the highest compression modulus is achieved when the load is orthogonal to the layer plane (C2 and C9 samples). However, this discrepancy in stiffness is more pronounced in TPU than in Reciflex. Specifically, orthogonally loaded TPU specimens are 7%–12% stiffer than parallelly loaded ones, whereas in Reciflex, they are 2%–13% stiffer. This phenomenon may be explained by the fact that, when the load is orthogonal to the infill lines, it compresses beads against each other, promoting the closure of voids within the samples. This results in higher resistance and highlights the importance of considering the interplay between infill alignment and loading direction in optimizing the compressive behaviour of ME components. A similar phenomenon is observed when comparing load cases with the load parallel to the layer plane and orthogonal to infill beads (C6 and C13). In these cases, because beads are compressed against each other, the computed stiffness is higher compared to when loads are parallel to both the layer plane and infill beads (samples C7 and C14).

Soon after being compressed to 70% of their initial height, cubic specimens regained a considerable portion of their original shape, and two weeks later, they exhibited nearly complete recovery, with all recoveries surpassing 90%. No significant differences were observed, except for a tendency towards reduced recovery with increasing extrusion temperature, particularly in Reciflex specimens. Furthermore, no height recovery was measured in specimens with [0°/0°] infill, in which the load is applied parallel to the infill beads, as these specimens sustained permanent damaged during the mechanical tests.

Figure 15 shows a representative example of damaged cubic specimens after compression, suggesting that their failure is likely due to delamination of layers combined with the buckling of infill beads.

Many studies have investigated the compression behaviour of 3D-printed TPU cellular structures (Dixit and Jain, 2022; León-Calero *et al.*, 2021; Nace *et al.*, 2021), but reports on their bulk properties are scarce. Table 7 summarizes the available literature on the compression properties of various types of 3D-printed TPUs and compares them with the results from this study. Both Reciflex and TPU 95A exhibit higher compressive

Figure 14 Average nominal stress–strain plots of specimens made with

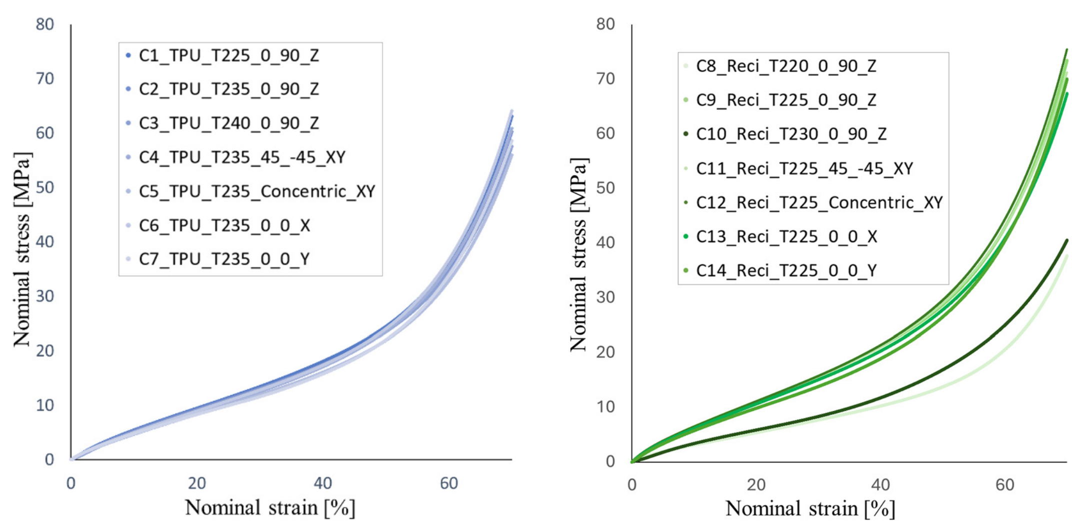

(a) (b)

Notes: (a) TPU 95A; (b) reciflex
Source: Figure by authors

Table 6 Compression results, including initial modulus, compressive stress at various strain levels and height recovery

Sample reference	$E_{1\%–20\%}$ [MPa]	$\sigma_{10\%}$ [MPa]	$\sigma_{20\%}$ [MPa]	$\sigma_{50\%}$ [MPa]	$\sigma_{70\%}$ [MPa]	R_e [%]
C1_TPU_T225_0_90_Z	46.3 ± 0.3	5.5 ± 0.1	9.5 ± 0.1	24.5 ± 0.3	63.2 ± 1.5	94 ± 0
C2_TPU_T235_0_90_Z	46.0 ± 1.1	5.4 ± 0.1	9.4 ± 0.2	23.9 ± 0.4	60.9 ± 0.9	94 ± 1
C3_TPU_T240_0_90_Z	45.1 ± 1.6	5.0 ± 0.4	9.1 ± 0.4	23.5 ± 0.2	57.6 ± 1.6	93 ± 1
C4_TPU_T235_45_−45_XY	42.1 ± 1.3	4.8 ± 0.2	8.7 ± 0.3	23.6 ± 0.7	61.0 ± 2.8	96 ± 2
C5_TPU_T235_Concentric_XY	40.4 ± 1.5	4.7 ± 0.2	8.4 ± 0.3	22.0 ± 0.9	56.0 ± 2.1	97 ± 1
C6_TPU_T235_0_0_X	43.2 ± 0.6	5.0 ± 0.1	8.9 ± 0.1	24.0 ± 0.4	64.2 ± 1.1	96 ± 0
C7_TPU_T235_0_0_Y	40.2 ± 1.9	4.8 ± 0.4	8.3 ± 0.4	22.0 ± 0.8	58.7 ± 0.6	–*
C8_Reci_T220_0_90_Z	25.8 ± 4.9	3.1 ± 0.5	5.4 ± 1.0	13.8 ± 2.1	37.7 ± 5.1	96 ± 0
C9_Reci_T225_0_90_Z	53.9 ± 1.8	6.4 ± 0.3	11.0 ± 0.4	28.8 ± 0.7	73.5 ± 1.4	93 ± 0
C10_Reci_T230_0_90_Z	29.1 ± 0.9	3.4 ± 0.1	5.9 ± 0.2	16.9 ± 0.2	40.6 ± 0.5	91 ± 1
C11_Reci_T225_45_−45_XY	52.7 ± 0.2	6.4 ± 0.1	10.9 ± 0.1	29.0 ± 0.3	71.3 ± 2.2	97 ± 0
C12_Reci_T225_Concentric_XY	52.8 ± 0.5	6.4 ± 0.1	11.1 ± 0.1	29.5 ± 0.3	75.5 ± 0.9	96 ± 1
C13_Reci_T225_0_0_X	51.1 ± 1.2	6.2 ± 0.2	10.6 ± 0.3	27.8 ± 0.9	67.4 ± 3.7	97 ± 2
C14_Reci_T225_0_0_Y	47.6 ± 0.7	5.8 ± 0.1	9.9 ± 0.2	26.5 ± 0.9	70.1 ± 5.0	–*

Note: *Recovery is not calculated because the samples were damaged
Source: Table by authors

properties compared to most TPUs, including TPU 95A tested under similar load conditions, such as in the study by León-Calero *et al.* (2021).

4. Conclusion

In this study, the authors explore the tensile strength and compressive behaviour of two ME-TPUs: TPU 95A from Ultimaker® and a recycled filament, Reciflex. The focus is on the influence of two processing parameters: extrusion temperature and infill strategy. Besides mechanical testing, thermal characterization of both materials was performed using DSC and TSDC techniques. Similar thermal responses were observed in both the raw filament and processed materials, suggesting that the ME process had little impact on their thermal characteristics. Furthermore, these tests allowed for the identification of the T_g and T_m, and the results align with available literature on ME-TPEs. The surface morphology of the specimens was analysed using SEM, which effectively allowed the quantification of void sizes within them. A simple analytical model, describing the infill bead as an ellipse constrained by the layer height and line width, correlated well with the actual void measurements.

The study finds that Reciflex exhibits greater stiffness than TPU 95A in both tensile and compressive tests. However, this recycled material is notably sensitive to slight variations in extrusion temperature. Producing complex structures using ME often requires a delicate balance of temperature, cooling and speed, which influence the heat applied to the filament. Consequently, the authors suggest that using recycled filaments like Reciflex requires careful consideration due to their potentially limited flexibility in production settings, which may pose challenges during production stages such as part design and slicing. Despite this, the mechanical properties of Reciflex closely align with those of TPU 95A, making it a promising alternative. However, further refinement and a deeper understanding of the material's characteristics and printability are needed.

The authors highlight the following key findings from the study:

- Higher extrusion temperatures, likely enhancing material flow, led to fewer voids and, consequently, higher cross-sectional SR.
- Most observed voids are triangular, except in specimens with a [45°/−45°] infill, which exhibited ovalized and larger voids. In some cases, these larger voids resulted from the merging of voids from consecutive layers.
- The highest average tensile strength (~38 MPa) was recorded in TPU 95A produced at 235°C with a [0°/90°] infill and in Reciflex at 225°C with a [0°/0°] infill. Although specimens with concentric infill showed high

Figure 15 Example of the failure behaviour of a compression specimen with [0°/0°] infill, where the load is applied parallel to the infill beads (C7 sample)

Source: Figure by authors

Table 7 Summary of compressive properties ME-TPUs available in the literature

Source	TPU type	Test speed [mm/min]	$E_{1\%–20\%}$ [MPa]	$\sigma_{10\%}$ [MPa]	$\sigma_{20\%}$ [MPa]	T_{ext} [°C]	Infill type	Load-layer
León-Calero *et al.* (2021)	PolyFlex 95A	10	18–31	1.8–2.6	~6.2	225	[0°/90°]	Ortg.
	Filaflex 95A	10	~32	~3.1	~6.4	225	[0°/90°]	Ortg.
	Filaflex 82A	10	11–17	1.1–1.5	3.1–3.4	230	[0°/90°]	Ortg.
	Filaflex 70A	10	5–11	~0.5	~1.1	235	[0°/90°]	Ortg.
	FlexiSmart 88A	10	13–27	1.3–2.3	~5.4	225	[0°/90°]	Ortg.
Petousis *et al.* (2023)	TPU (Ravago Petrokimya)	1.3–200	100–140	10–15	22–29	215	NA	NA
This research	Ultimaker TPU 95A	2	45–46	5.0–5.5	9.0–9.5	225/235/240	[0°/90°]	Ortg.
			40–43	4.7–5.0	8.3–8.9	235	[Concentric]; [45°/−45°]; [0°/0°]	Prll.
	Recreus Reciflex		26–54	3.1–6.4	5.4–11.0	220/225/230	[0°/90°]	Ortg.
			47–53	5.8–6.4	9.9–11.1	225	[Concentric]; [45°/−45°]; [0°/0°]	Prll.

Notes: NA = not available; Ortg: orthogonal; Prll = parallel
Source: Table by authors

initial stiffness, their strength and stretchability were significantly lower due to macroscopic defects. Generally, higher tensile properties are associated with material beads deposited parallel to the load direction.

- Variations in infill showed a weak correlation with computed SR values for both materials concerning tensile strength and stretchability. However, a slight correlation between stiffness and computed SR was observed in TPU.
- A positive correlation between greater SRs and improvements in strength and stretchability was observed with increased extrusion temperatures, particularly in Reciflex.
- In compression tests, orthogonally loaded TPU specimens were 7%–12% stiffer than parallelly loaded ones, whereas Reciflex specimens were 2%–13% stiffer. This increased stiffness is likely due to beads being compressed against each other, helping to close voids within the samples.
- Two weeks after undergoing compression to 70% of their original height, most specimens exhibited nearly complete shape recovery, except those with a [0°/0°] infill, where the load was applied parallel to the infill beads, because these were permanently damaged during the tests.
- The most consistent mechanical properties were achieved at extrusion temperatures of 235°C and 240°C for TPU and 225°C for Reciflex. Therefore, these are the extrusion temperatures that the authors recommend when working with these materials.

Acknowledgements

This work was supported by Fundacaô õ para a Cien̂cia e a Tecnologia (FCT) through IDMEC, under LAETA Base Funding (DOI: 10.54499/UIDB/50022/2020), through CEGIST (DOI: 10.54499/UIDB/00097/2020), through CQE (DOI: 10.54499/UIDB/00100/2020 and DOI: 10.54499/UIDP/00100/2020) and through IMS (DOI: 10.54499/LA/P/0056/2020). Manuel Sardinha acknowledges FCT, for his PhD research grant, https://doi.org/10.54499/2021.04919.BD.

Declaration of competing interest: The authors declare no conflicts of interest.

Credit authorship contribution statement: Manuel Sardinha, Conceptualization, Methodology, Investigation, Formal analysis, Writing – Original Draft. *Luís Ferreira*, Investigation. *Hermínio P. Diogo*, Investigation, Writing – review and editing. *T.R.P. Ramos*, Visualization, Writing – review and editing. *Luís Reis*, Conceptualization, Resources, Writing – review and editing. *M. Fátima Vaz*, Conceptualization, Resources, Writing – review and editing, Supervision.

Declaration of generative AI and AI-assisted technologies in the writing process: During the preparation of this work, the authors used ChatGPT 4.0 to improve the language level. Included content was thoroughly reviewed and edited as needed and the authors take full responsibility for the publication.

References

Abdulhameed, O., Al-Ahmari, A., Ameen, W. and Mian, S.H. (2019), "Additive manufacturing: challenges, trends, and applications", *Advances in Mechanical Engineering*, Vol. 11 No. 2, pp. 1-27, doi: 10.1177/1687814018822880.

Adibeig, M.R., Saeimi-Sadigh, M.A., Vakili-Tahami, F., Karimani, M.R. and Marami, G. (2023), "Quasi-static simulation and fatigue life estimation of fused filament fabrication of polylactic acid specimens using finite element method", *Journal of Manufacturing Processes*, Elsevier Ltd, Vol. 106, pp. 202-213, doi: 10.1016/j.jmapro.2023.09.071.

Ajinjeru, C., Kishore, V., Liu, P., Hassen, A.A., Lindahl, J., Kunc, V. and Duty, C. (2017), ""Rheological evaluation of high temperature polymers to identify successful extrusion parameters", *Proceedings of the 28th Annual International Solid Freeform Fabrication Symposium*, *University of TX at Austin*, pp. 485-494.

Akhoundi, B. and Behravesh, A.H. (2019), "Effect of filling pattern on the tensile and flexural mechanical properties of

FDM 3D printed products", *Experimental Mechanics*, Vol. 59 No. 6, pp. 883-897, doi: 10.1007/s11340-018-00467-y.
Altıparmak, S.C., Yardley, V.A., Shi, Z. and Lin, J. (2022), "Extrusion-based additive manufacturing technologies: state of the art and future perspectives", *Journal of Manufacturing Processes*, Elsevier Ltd, 1 November, Vol. 83, doi: 10.1016/j.jmapro.2022.09.032.
Arifvianto, B., Nur Iman, T., Tulung Prayoga, B., Dharmastiti, R., Agus Salim, U. and Mahardika, M. (2021), "Tensile properties of the FFF-processed thermoplastic polyurethane (TPU) elastomer", *The International Journal of Advanced Manufacturing Technology*, Vol. 117 Nos 5/6, pp. 1709-1719, doi: 10.1007/s00170-021-07712-0.
Armstrong, A., Kabir, S.M.F., Mathur, K. and Seyam, A.-F. M. (2023), "3D printing, a road to sustainable fashion", *Novel Sustainable Process Alternatives for the Textiles and Fashion Industry. Sustainable Textiles: Production, Processing, Manufacturing & Chemistry*, Springer, pp. 1-27, doi: 10.1007/978-3-031-35451-9_1.
ASTM (2014), "D638-14 standard test method for tensile properties of plastics", doi: 10.1520/D0638-14.
ASTM (2015), "D 3418-15 standard test method for transition temperatures and enthalpies of fusion and crystallization of polymers by differential scanning calorimetry".
ASTM (2016), "D412 - Standard test methods for vulcanized rubber and thermoplastic elastomers— tension".
Awasthi, P. and Banerjee, S.S. (2021), "Fused deposition modeling of thermoplastic elastomeric materials: Challenges and opportunities", *Additive Manufacturing*, Elsevier B.V, Vol. 46, doi: 10.1016/j.addma.2021.102177.
Babu, R.R. and Naskar, K. (2010), "Recent developments on thermoplastic elastomers by dynamic vulcanization", *Advanced Rubber Composites*, pp. 219-247, doi: 10.1007/12_2010_97.
Badini, S., Graziosi, S., Carboni, M., Regondi, S. and Pugliese, R. (2024), "Sustainable 3D printing with recycled tire rubber-based filaments: an investigation of process parameters and mechanical behaviour", *Rapid Prototyping Journal*, Vol. 30 No. 3, doi: 10.1108/RPJ-08-2023-0309.
Bellehumeur, C., Li, L., Sun, Q. and Gu, P. (2004), "Modeling of bond formation between polymer filaments in the fused deposition modeling process", *Journal of Manufacturing Processes*, Elsevier BV, Vol. 6 No. 2, pp. 170-178, doi: 10.1016/S1526-6125(04)70071-7.
Bin Samsuri, A. (2017), "Degradation of natural rubber and synthetic elastomers", *Reference Module in Materials Science and Materials Engineering*, Vol. 3, pp. 2407-2438.
Coasey, K., Hart, K.R., Wetzel, E., Edwards, D. and Mackay, M.E. (2020), "Nonisothermal welding in fused filament fabrication", *Additive Manufacturing*, Elsevier B.V, Vol. 33, doi: 10.1016/j.addma.2020.101140.
Coogan, T.J. and Kazmer, D.O. (2017), "Bond and part strength in fused deposition modeling", *Rapid Prototyping Journal*, Vol. 23 No. 2, pp. 414-422, doi: 10.1108/RPJ-03-2016-0050.
Coogan, T.J. and Kazmer, D.O. (2020), "Prediction of interlayer strength in material extrusion additive manufacturing", *Additive Manufacturing*, Elsevier B.V, Vol. 35, doi: 10.1016/j.addma.2020.101368.
Das, A., Gilmer, E.L., Biria, S. and Bortner, M.J. (2021), "Importance of polymer rheology on material extrusion additive manufacturing: correlating process physics to print properties", *ACS Applied Polymer Materials*, Vol. 3 No. 3, pp. 1218-1249, doi: 10.1021/acsapm.0c01228.
Datta, J. and Kasprzyk, P. (2018), "Thermoplastic polyurethanes derived from petrochemical or renewable resources: a comprehensive review", *Polymer Engineering & Science*, Vol. 58 No. S1, doi: 10.1002/pen.24633. 1 May.
Diogo, H.P., Viciosa, M.T. and Ramos, J.J.M. (2016), "Differential scanning calorimetry and thermally stimulated depolarization currents study on the molecular dynamics in amorphous fenofibrate", *Thermochimica Acta*, Elsevier, Vol. 623, pp. 29-35, doi: 10.1016/J.TCA.2015.11.012.
Dixit, N. and Jain, P.K. (2022), "Effect of fused filament fabrication process parameters on compressive strength of thermoplastic polyurethane and polylactic acid lattice structures", *Journal of Materials Engineering and Performance*, Springer, Vol. 31 No. 7, pp. 5973-5982, doi: 10.1007/s11665-022-06664-0.
Eiliat, H. and Urbanic, R.J. (2018), "Minimizing voids for a material extrusion-based process", *Rapid Prototyping Journal*, Vol. 24 No. 2, pp. 485-500, doi: 10.1108/RPJ-05-2017-0092.
Elhattab, K., Bhaduri, S.B. and Sikder, P. (2022), "Influence of fused deposition modelling nozzle temperature on the rheology and mechanical properties of 3D printed β-tricalcium phosphate (TCP)/polylactic acid (PLA) composite", *Polymers, MDPI*, Vol. 14 No. 6, doi: 10.3390/polym14061222.
Ferraris, E., Zhang, J. and Van Hooreweder, B. (2019), "Thermography based in-process monitoring of fused filament fabrication of polymeric parts", *CIRP Annals*, Elsevier USA, Vol. 68 No. 1, pp. 213-216, doi: 10.1016/j.cirp.2019.04.123.
Frick, A. and Rochman, A. (2004), "Characterization of TPU-elastomers by thermal analysis (DSC)", *Polymer Testing*, Vol. 23 No. 4, pp. 413-417, doi: 10.1016/j.polymertesting.2003.09.013.
Garzon-Hernandez, S., Garcia-Gonzalez, D., Jérusalem, A. and Arias, A. (2020), "Design of FDM 3D printed polymers: an experimental-modelling methodology for the prediction of mechanical properties", *Materials and Design*, Elsevier Ltd, Vol. 188, doi: 10.1016/j.matdes.2019.108414.
Geng, T., Xiao, H.C., Wang, X.C., Liu, C.T., Wu, L., Guo, Y. G., Dong, B.B., *et al.* (2023), "The study on the morphology and compression properties of microcellular TPU/nanoclay tissue scaffolds for potential tissue engineering applications", *Polymers, Multidisciplinary Digital Publishing Institute (MDPI)*, Vol. 15 No. 17, doi: 10.3390/polym15173647.
Gibson, I., Rosen, D. and Stucker, B. (2014), *Additive Manufacturing Technologies: 3D Printing, Rapid Prototyping, and Direct Digital Manufacturing*, 2nd ed., Springer.
Hohimer, C., Christ, J., Aliheidari, N., Mo, C. and Ameli, A. (2017), "3D printed thermoplastic polyurethane with isotropic material properties", Behavior and Mechanics of Multifunctional Materials and Composites 2017, Vol. 10165, *SPIE*, p. 1016511, doi: 10.1117/12.2259810.
Kartsovnik, V.I. (2022), "Relationship between the deformation processes occurring in rubbers and their

molecular structure: (structure of rubbers under strain)", *Journal of Macromolecular Science, Part B: Physics*, Taylor and Francis Ltd, Vol. 61 No. 3, pp. 324-343, doi: 10.1080/00222348.2021.2005914.

Kasmi, S., Ginoux, G., Labbé, E. and Alix, S. (2022), "Multi-physics properties of thermoplastic polyurethane at various fused filament fabrication parameters", *Rapid Prototyping Journal*, Vol. 28 No. 5, pp. 895-906, doi: 10.1108/RPJ-08-2021-0214.

Kechagias, J.D., Vidakis, N. and Petousis, M. (2021), "Parameter effects and process modeling of FFF-TPU mechanical response", *Materials and Manufacturing Processes*, Taylor and Francis Ltd, Vol. 38 No. 3, doi: 10.1080/10426914.2021.2001523.

Koch, C., Van Hulle, L. and Rudolph, N. (2017), "Investigation of mechanical anisotropy of the fused filament fabrication process via customized tool path generation", *Additive Manufacturing*, Elsevier B, Vol. 16, pp. 138-145, doi: 10.1016/j.addma.2017.06.003.

Kucherskii, A.M. (2003), "New characteristic of tensile stress-strain properties in rubbers", *Polymer Testing*, Vol. 22 No. 5, pp. 503-507, doi: 10.1016/S0142-9418(02)00113-7.

Lee, J.Y., An, J. and Chua, C.K. (2017), "Fundamentals and applications of 3D printing for novel materials", *Applied Materials Today*, Elsevier Ltd, 1 June, Vol. 7, doi: 10.1016/j.apmt.2017.02.004.

León-Calero, M., Reyburn Valés, S.C., Marcos-Fernández, Á. and Rodríguez-Hernandez, J. (2021), "3D printing of thermoplastic elastomers: role of the chemical composition and printing parameters in the production of parts with controlled energy absorption and damping capacity", *Polymers, MDPI*, Vol. 13 No. 20, doi: 10.3390/polym13203551.

Lin, T.A., Lin, J.H. and Bao, L. (2020), "Polypropylene/thermoplastic polyurethane blends: Mechanical characterizations, recyclability and sustainable development of thermoplastic materials", *Journal of Materials Research and Technology*, Elsevier Editora Ltda, Vol. 9 No. 3, pp. 5304-5312, doi: 10.1016/j.jmrt.2020.03.056.

Luo, C. (2020), "Modeling the temperature profile of an extrudate in material extrusion additive manufacturing", *Materials Letters*, Elsevier B.V, Vol. 270, doi: 10.1016/j.matlet.2020.127742.

Mackay, M.E. (2018), "The importance of rheological behavior in the additive manufacturing technique material extrusion", *Journal of Rheology, Society of Rheology*, Vol. 62 No. 6, pp. 1549-1561, doi: 10.1122/1.5037687.

Mian, S.H., Abouel Nasr, E., Moiduddin, K., Saleh, M. and Alkhalefah, H. (2024), "An insight into the characteristics of 3D printed polymer materials for orthoses applications: Experimental study", *Polymers, Multidisciplinary Digital Publishing Institute (MDPI*, Vol. 16 No. 3, doi: 10.3390/polym16030403.

Nace, S.E., Tiernan, J., Holland, D. and Ni Annaidh, A. (2021), "A comparative analysis of the compression characteristics of a thermoplastic polyurethane 3D printed in four infill patterns for comfort applications", *Rapid Prototyping Journal*, Vol. 27 No. 11, pp. 24-36, doi: 10.1108/RPJ-07-2020-0155.

Papazetis, G. and Vosniakos, G.C. (2019), "Mapping of deposition-stable and defect-free additive manufacturing via material extrusion from minimal experiments", *The International Journal of Advanced Manufacturing Technology*, Vol. 100 Nos 9/12, pp. 2207-2219, doi: 10.1007/s00170-018-2820-1.

Peng, F., Vogt, B.D. and Cakmak, M. (2018), "Complex flow and temperature history during melt extrusion in material extrusion additive manufacturing", *Additive Manufacturing*, Elsevier B.V, Vol. 22, pp. 197-206, doi: 10.1016/j.addma.2018.05.015.

Petousis, M., Ntintakis, I., David, C., Sagris, D., Nasikas, N. K., Korlos, A., Moutsopoulou, A., *et al.* (2023), "A coherent assessment of the compressive strain rate response of PC, PETG, PMMA, and TPU thermoplastics in MEX additive manufacturing", *Polymers, Multidisciplinary Digital Publishing Institute (MDPI*, Vol. 15 No. 19, doi: 10.3390/polym15193926.

Qamar Tanveer, M., Mishra, G., Mishra, S. and Sharma, R. (2022), "Effect of infill pattern and infill density on mechanical behaviour of FDM 3D printed parts- a current review", *Materials Today: Proceedings*, Elsevier Ltd, Vol. 62, pp. 100-108, doi: 10.1016/j.matpr.2022.02.310.

Recreus (2022), "Reciflex", available at: https://recreus.com/gb/filaments/4-reciflex.html (accessed 15 October 2024).

Salem, M.E.M., Wang, Q., Wen, R. and Xiang, M. (2018), "Design and characterization of soft pneumatic actuator for universal robot gripper", 2018 International Conference on Control and Robots (ICCR), pp. 6-10, doi: 10.1109/ICCR.2018.8534483.

Sardinha, M., Fátima Vaz, M., Ramos, T.R.P. and Reis, L. (2023), "Design, properties, and applications of non-pneumatic tires: a review", *Proceedings of the Institution of Mechanical Engineers, Part L: Journal of Materials: Design and Applications*, SAGE Publications Ltd, Vol. 237 No. 11, doi: 10.1177/14644207231177302.

Sardinha, M., Ferreira, L., Ramos, T., Reis, L. and Vaz, M.F. (2024), "Challenges on extrusion-based additive manufacturing of thermoplastic polyurethane", *Engineering Manufacturing Letters*, Vol. 2 No. 1, pp. 45-52, doi: 10.24840/2795-5168_002-001_2675.

Sardinha, M., Reis, L., Ramos, T. and Vaz, M.F. (2022), "Non-pneumatic tire designs suitable for fused filament fabrication: an overview", *Procedia Structural Integrity*, Vol. 42, pp. 1098-1105, doi: 10.1016/j.prostr.2022.12.140.

Sean Teller (2019), "High strain rate testing of elastomers and thermoplastic elastomers", *Rubber World*, Vol. 259 No. 4, pp. 40-43.

Steuben, J., Van Bossuyt, D.L. and Turner, C. (2015), "Design for fused filament fabrication additive manufacturing", Proceedings of the ASME Design Engineering Technical Conference, Vol. 4, *American Society of Mechanical Engineers (ASME)*, doi: 10.1115/DETC2015-46355.

Sun, X., Mazur, M. and Cheng, C.T. (2023), "A review of void reduction strategies in material extrusion-based additive manufacturing", *Additive Manufacturing*, Elsevier B.V, 5 April, Vol. 67, doi: 10.1016/j.addma.2023.103463.

Tao, Y., Kong, F., Li, Z., Zhang, J., Zhao, X., Yin, Q., Xing, D., *et al* (2021), "A review on voids of 3D printed parts by fused filament fabrication", *Journal of Materials Research and Technology, Elsevier Editora Ltda*, 1 November, Vol. 15, doi: 10.1016/j.jmrt.2021.10.108.

Tao, Y., Ren, M., Zhang, H. and Peijs, T. (2021), "Recent progress in acoustic materials and noise control strategies – a review", *Applied Materials Today*, Elsevier Ltd, 1 September, Vol. 24, doi: 10.1016/j.apmt.2021.101141.

Tofail, S., A.M., Koumoulos, E.P., Bandyopadhyay, A., Bose, S., O'Donoghue, L. and Charitidis, C. (2018), "Additive manufacturing: scientific and technological challenges, market uptake and opportunities", *Materials Today*, Elsevier B.V, 1 January, Vol. 21 No. 1, doi: 10.1016/j.mattod.2017.07.001.

Treloar, L.R.G. (1975), "The physics of rubber elasticity, in oxford classic texts in the physical sciences".

UltiMaker (2022), "UltiMaker TPU 95A TDS", available at: https://support.makerbot.com/s/article/1667410781018 (accessed 15 October 2024).

UltiMaker (2024), "How to print with UltiMaker TPU 95A", available at: https://support.makerbot.com/s/article/1667337612195 (accessed 25 January 2024).

Vidakis, N., Petousis, M., Korlos, A., Velidakis, E., Mountakis, N., Charou, C. and Myftari, A. (2021), "Strain rate sensitivity of polycarbonate and thermoplastic polyurethane for various 3d printing temperatures and layer heights", *Polymers, MDPI AG*, Vol. 13 No. 16, doi: 10.3390/polym13162752.

Wach, R.A., Wolszczak, P. and Adamus-Wlodarczyk, A. (2018), "Enhancement of mechanical properties of FDM-PLA parts via thermal annealing", *Macromolecular Materials and Engineering*, Vol. 303 No. 9, doi: 10.1002/mame.201800169.

Wang, K., Engelbrecht, K. and Bahl, C.R.H. (2023), "Additive manufactured thermoplastic elastomers for low-stress driven elastocaloric cooling", *Applied Materials Today*, Elsevier Ltd, Vol. 30, doi: 10.1016/j.apmt.2022.101711.

Wickramasinghe, S., Do, T. and Tran, P. (2020), "FDM-Based 3D printing of polymer and associated composite: a review on mechanical properties, defects and treatments", *Polymers, MDPI AG, 1*, Vol. 12 No. 7, doi: 10.3390/polym12071529.

Wu, P., Qian, C. and Okwudire, C.E. (2024), "Design, modeling and feedforward control of a hybrid extruder for material extrusion additive manufacturing", *Additive Manufacturing*, Elsevier B.V, Vol. 92, doi: 10.1016/j.addma.2024.104378.

Xiao, J. and Gao, Y. (2017), "The manufacture of 3D printing of medical grade TPU", *Progress in Additive Manufacturing, Springer*, Vol. 2 No. 3, pp. 117-123, doi: 10.1007/s40964-017-0023-1.

Xu, T., Shen, W., Lin, X. and Xie, Y.M. (2020), "Mechanical properties of additively manufactured thermoplastic polyurethane (TPU) material affected by various processing parameters", *Polymers, MDPI AG*, Vol. 12 No. 12, pp. 1-16, doi: 10.3390/polym12123010.

Zhou, L.Y., Fu, J. and He, Y. (2020), "A review of 3D printing technologies for soft polymer materials", *Advanced Functional Materials*, 1 July, Vol. 30 No. 28, doi: 10.1002/adfm.202000187.

Zia, K.M., Bhatti, H.N. and Ahmad Bhatti, I. (2007), "Methods for polyurethane and polyurethane composites, recycling and recovery: a review", *Reactive and Functional Polymers*, Vol. 67 No. 8, doi: 10.1016/j.reactfunctpolym.2007.05.004.

Supplementary material

The supplementary material for this article can be found online.

Corresponding author

Manuel Sardinha can be contacted at: manuel.r.sardinha@tecnico.ulisboa.pt